Obtaining efficient thermal engines from interacting Brownian particles under time-periodic drivings

Iago N. Mamede,[1] Pedro E. Harunari,[1,2] Bruno A. N. Akasaki,[1] Karel Proesmans,[2,3,4] and C. E. Fiore[1]

[1]*Instituto de Física da Universidade de São Paulo, 05314-970 São Paulo, Brazil*

[2]*Complex Systems and Statistical Mechanics, Physics and Materials Science Research Unit, University of Luxembourg, L-1511 Luxembourg, Luxembourg*

[3]*Hasselt University, B-3590 Diepenbeek, Belgium*

[4]*Niels Bohr Institute, University of Copenhagen, Blegdamsvej 17, Copenhagen, Denmark*

(Received 18 October 2021; accepted 18 January 2022; published 4 February 2022)

We introduce an alternative route for obtaining reliable cyclic engines, based on two interacting Brownian particles under time-periodic drivings which can be used as a work-to-work converter or a heat engine. Exact expressions for the thermodynamic fluxes, such as power and heat, are obtained using the framework of stochastic thermodynamic. We then use these exact expression to optimize the driving protocols with respect to output forces, their phase difference. For the work-to-work engine, they are solely expressed in terms of Onsager coefficients and their derivatives, whereas nonlinear effects start to play a role since the particles are at different temperatures. Our results suggest that stronger coupling generally leads to better performance, but careful design is needed to optimize the external forces.

DOI: 10.1103/PhysRevE.105.024106

I. INTRODUCTION

Small-scale engines operating out of equilibrium have received significantly increasing attention in the last years, especially because several processes in nature (mechanical, biological, chemical and others) are related to some kind of energy conversion (e.g., mechanical into chemical and vice versa) [1–3]. The constant fluctuating flow of energy constitutes a fundamental feature fueling the operation of nonequilibrium engines which is well described by the framework of stochastic thermodynamics [1].

Entropy production plays a fundamental role in nonequilibrium thermodynamics. It satisfies fluctuation theorems [4,5], general bounds also known as thermodynamic uncertainty relations (TURs) [6–13] and general trade-offs between power, efficiency, and dissipation [14,15]. Here we look at a case study of a cyclic heat engine in which the nonequilibrium features are due to distinct thermal reservoirs and time-dependent external forces. We focus on systems with time-dependent driving for two reasons: first, time-dependent driving is arguably the simplest way to drive Brownian particles out of equilibrium [16,17] and second, systems with time-dependent driving have been shown to outperform steady-state systems [18–20].

Brownian particles are often at the core of nanoscaled heat engines [16,17,21–28]. Most of them are based on single-particle engines and have been studied for theoretical [29–38] and experimental [21,39,40] settings. On the other hand, the number of studies on the thermodynamic properties of interacting chains of particles are limited and often constrained to time-independent driving [28,41]. The scarcity of results [42], together the richness of such system, raises distinct and relevant questions about the interaction contribution to the performance, the interplay between interaction and driving forces, and choice of protocol optimization. The last is a field in itself with many recent works focusing on the optimization of distinct engines in terms of efficiency and/or power [32,43–46].

In this work we conciliate above issues by introducing an interacting version of the underdamped Brownian duet [47], in which each particle is subject to a distinct thermal bath and driving force. The existence of distinct parameters (interaction between particles, strength of forces, phase difference, and frequency) provides several routes for tackling optimization that will be analyzed using the framework of stochastic thermodynamics. In order to exploit the role of distinct parameters, analysis will be considered for the (simplest) system composed of two Brownian particles. Two different situations will be addressed. Initially, we consider the case in which the thermal baths have the same temperature (interacting particle work-to-work converter) [17], in which maximizations are solely expressed in terms of Onsager coefficients and their derivatives. We then advance beyond the work-to-work converter by including a temperature difference between thermal baths and general predictions are obtained for distinct set of temperatures.

Distinct types of optimization will be introduced and analyzed: maximization of output power and efficiency with respect to the output forces, phase difference between external forces, and both of them. We obtain expressions for efficiency, power, and the optimization parameters in both regimes of maximum efficiency and maximum power. Results reveal that the coupling parameter is found to monotonically enhance both efficiency and/or power, highlighting the importance of

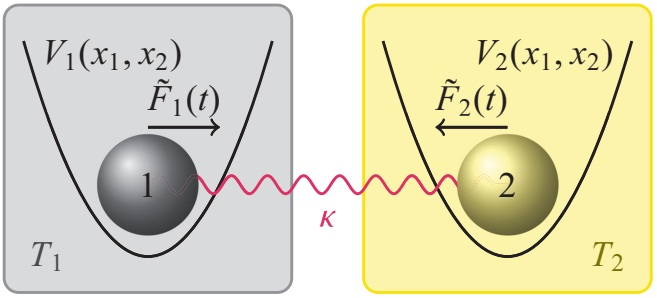

FIG. 1. Scheme of the two-particle Brownian engine. Each particle is subject to a temperature T_i, potential V_i, and time-dependent external force $\tilde{F}_i$, and both are coupled by a harmonic interaction with parameter κ.

the interaction between particles for the machine operation. Conversely, the frequency, lag, and input forces have specific optimal values and, in general, regimes of maximum efficiency and maximum power.

The paper is structured as follows: in Sec. II we introduce the model and the main expressions for relevant quantities. In Sec. III we analyze the engine performance for distinct regime operations. Conclusions are drawn in Sec. IV.

II. THERMODYNAMICS OF INTERACTING BROWNIAN ENGINES

The model is composed by two interacting underdamped Brownian particles with equal mass m, each one subject to a distinct external force and placed in contact with a thermal bath of temperature T_i, $i = \{1, 2\}$, as exemplified in Fig. 1. Their positions and velocities, x_i and v_i, evolve in time according to the following set of Langevin equations:

$$\frac{dv_1}{dt} = \frac{1}{m}F_1^*(x_1, x_2) + \frac{1}{m}\tilde{F}_1(t) - \gamma v_1 + \zeta_1, \tag{1}$$

$$\frac{dv_2}{dt} = \frac{1}{m}F_2^*(x_1, x_2) + \frac{1}{m}\tilde{F}_2(t) - \gamma v_2 + \zeta_2, \tag{2}$$

and

$$\frac{dx_1}{dt} = v_1, \quad \frac{dx_2}{dt} = v_2, \tag{3}$$

respectively. There are eight forces acting on the system: two forces $F_i^*(x_1, x_2)$, related to the harmonic potentials and the interaction between particles, two external driving components $\tilde{F}_i(t)$, friction forces $-\gamma v_i$ (with γ denoting the friction parameter) and stochastic forces $\zeta_i(t)$. The former can be written as the derivative of a potential V_i given by $F_i^*(x_1, x_2) = -\partial V_i/\partial x_i$, whereas the stochastic forces are described as a white noise: $\langle\zeta_i(t)\rangle = 0$ and $\langle\zeta_i(t)\zeta_j(t')\rangle = 2\gamma k_B T_i \delta_{ij}\delta(t - t')/m$. The above set of Langevin equations are associated with the probability distribution $P(x_1, x_2, v_1, v_2, t)$ having its time evolution governed by Fokker-Planck-Kramers (FPK) equation:

$$\frac{\partial P}{\partial t} = -\sum_{i=1}^{2}\left\{v_i\frac{\partial P}{\partial x_i} + [F_i^* + \tilde{F}_i(t)]\frac{\partial P}{\partial v_i} + \frac{\partial J_i}{\partial v_i}\right\}, \tag{4}$$

where

$$J_i = -\gamma v_i P - \frac{\gamma k_B T_i}{m}\frac{\partial P}{\partial v_i}. \tag{5}$$

If the temperatures of both particles are equal and the external forces are absent, the probability distribution approaches for large times the Gibbs equilibrium distribution, $P^{\rm eq}(x_1, x_2, v_1, v_2) \propto e^{-E/k_B T}$, where E is the total energy of the system. From now on, we shall consider harmonic potentials $V_i = k_i x_i^2/2 + \kappa(x_i - x_j)^2/2$, whose associated forces read $F_i^* = -kx_i - \kappa(x_i - x_j)$. The time evolution of a generic average $\langle x_i^n v_j^m\rangle$ can be obtained from the FPK equation (4) and performing appropriate partial integrations by assuming that $P(x_1, x_2, v_1, v_2, t)$ and its derivatives vanish when x_i or v_i approaches $\pm\infty$. More specifically, we are interested in obtaining expressions for thermodynamic quantities, such as the heat exchanged between particle i and the reservoir and the work rate performed by each external force over its particle. Their expressions can be obtained from the time evolution of mean energy $\langle E\rangle$ together the FPK equation and assumes a form consistent with the first law of thermodynamics [1,48,49]:

$$\frac{d\langle E\rangle}{dt} = -\sum_{i=1}^{2}(\dot{W}_i + \dot{Q}_i), \tag{6}$$

where $\dot{W}_i$ is work done over particle i, due to the external force $\tilde{F}_i(t)$,

$$\dot{W}_i = -m\tilde{F}_i(t)\langle v_i\rangle, \tag{7}$$

and $\dot{Q}_i$ is the heat delivered to reservoir i. An expression for the heat can be derived from the above two equations:

$$\dot{Q}_i = \gamma\left(m\langle v_i^2\rangle - k_B T_i\right). \tag{8}$$

Similarly, the time evolution of system entropy $S = -k_B\langle\ln P(x_1, x_2, v_1, v_2)\rangle$ is the difference between entropy production rate σ and entropy flux rate Φ to or from the system to or from the thermal reservoir given by [1,48,49]

$$\sigma = \frac{m}{\gamma}\sum_{i=1}^{2}\frac{1}{T_i}\int\frac{J_i^2}{P}\,dx_1\,dx_2\,dv_1\,dv_2 \tag{9}$$

and

$$\Phi = -\sum_{i=1}^{2}\frac{m}{T_i}\int v_i J_i\,dx_1\,dx_2\,dv_1\,dv_2, \tag{10}$$

respectively. Note that $\sigma \geqslant 0$ (as expected), whereas Φ can be conveniently rewritten in terms of the ratio between $\dot{Q}_i$ and the temperature T_i:

$$\Phi = \sum_i \gamma\left(\frac{m\langle v_i^2\rangle}{T_i} - k_B\right) = \sum_{i=1}^{2}\frac{\dot{Q}_i}{T_i}. \tag{11}$$

It is convenient to relate averages $\langle v_i\rangle$ and $\langle v_i^2\rangle$ by means their covariances $b_{ij}^{vv}(t) \equiv \langle v_i v_j\rangle(t) - \langle v_i\rangle(t)\langle v_j\rangle(t)$. For simplifying matters, from now on we set $m = k_B = 1$. Due to the interaction between particles, $b_{ij}^{vv}(t)$ also depends on covariances $b_{ij}^{xx}(t)$ and $b_{ij}^{xv}(t)$ (x and v attempting to show the position and velocity of the ith and jth particles, respectively). Their time evolutions are straightforwardly obtained from Eq. (4), whose expression for b_{11}^{vv} is given by

$$b_{11}^{vv} = \frac{T_1 + T_2}{2} + \frac{(T_1 - T_2)}{2}\frac{\gamma^2(\kappa + k)}{[\kappa^2 + \gamma^2(\kappa + k)]}, \tag{12}$$

and b_{22}^{vv} is obtained just by exchanging $1 \leftrightarrow 2$.

A. Periodically driving forces

Having obtained the general expressions for a chain of two interacting particles, we are now in position to get expressions in the presence of external forces. Our aim is to study the effect that interactions have on the performance of an engine. To do this, we will focus on the simplest case in which particles are subject to harmonic time-dependent forces $\tilde{F}_i(t)$ of different amplitude, same frequency ω, but with a lag δ between them [17,42,47,50]:

$$\tilde{F}_1(t) = X_1 \cos(\omega t) \tag{13}$$

and

$$\tilde{F}_2(t,\delta) = X_2 \cos[\omega(t-\delta)], \tag{14}$$

respectively. The system will relax to a time-periodic steady state with $\overline{\dot{Q}}_1 + \overline{\dot{Q}}_2 = -(\overline{\dot{W}}_1 + \overline{\dot{W}}_2)$, where each mean work $\overline{\dot{W}}_i$ and heat $\overline{\dot{Q}}_i$ are given by

$$\overline{\dot{W}}_i = -\frac{\omega}{2\pi}\int_0^{2\pi/\omega} \tilde{F}_i(t)\langle v_i\rangle(t)\,dt \tag{15}$$

and

$$\overline{\dot{Q}}_i = \frac{\omega\gamma}{2\pi}\int_0^{2\pi/\omega} \langle v_i\rangle^2\,dt - \overline{\kappa}(T_i - T_j), \tag{16}$$

respectively, where $\overline{\kappa}$ is the thermal conduction given by $\overline{\kappa} = \gamma\kappa^2/[2\kappa^2 + 2\gamma^2(\kappa + k)]$ [48,51]. Giving that Eqs. (9) and (11) are equal in the NESS, the steady entropy production over a cycle is promptly obtained from Eq. (11) and can be related to the average work and heat according to the expression

$$\overline{\sigma} = \frac{4T^2}{4T^2 - \Delta T^2}\left[-\frac{1}{T}(\overline{\dot{W}}_1 + \overline{\dot{W}}_2) + (\overline{\dot{Q}}_1 - \overline{\dot{Q}}_2)\frac{\Delta T}{2T^2}\right], \tag{17}$$

where $T = (T_1 + T_2)/2$ and $\Delta T = T_2 - T_1$. It can also be viewed as sum of two components: $\overline{\sigma} = \Phi_T + \overline{\Phi}_f$, where the former, Φ_T, due to the difference of temperatures is given by

$$\Phi_T = \frac{4\overline{\kappa}\Delta T^2}{4T^2 - \Delta T^2}, \tag{18}$$

and the latter, due to the external forces, is given by

$$\overline{\Phi}_f = \tilde{L}_{11}X_1^2 + (\tilde{L}_{12} + \tilde{L}_{21})X_1X_2 + \tilde{L}_{22}X_2^2, \tag{19}$$

respectively. Above expressions are exact and hold beyond linear regime (large forces and/or large difference of temperatures) between thermal baths. In order to relate them with thermodynamic fluxes and forces, we are going to perform the analysis of a small temperature difference ΔT between thermal baths. In such case, we introduce the forces $f_1 = X_1/T$, $f_2 = X_2/T$ and $f_T = \Delta T/T^2$, in such a way that

$$\overline{\sigma} \approx J_1 f_1 + J_2 f_2 + J_T f_T, \tag{20}$$

where flux i ($i = 1, 2$ or T) is associated with force f_i and given by the expressions $\overline{\dot{W}}_1 = -TJ_1f_1$, $\overline{\dot{W}}_2 = -TJ_2f_2$ and $\overline{\dot{Q}}_1 - \overline{\dot{Q}}_2 = 2J_Tf_T$. From them, one can obtain Onsager coefficients $J_1 = L_{11}f_1 + L_{12}f_2$, $J_2 = L_{21}f_1 + L_{22}f_2$ and $J_T = L_{TT}f_T$, whose main expressions are listed below:

$$L_{11} = L_{22} = \left(\frac{T\gamma\omega^2}{2}\right)\frac{\gamma^2\omega^2 + [\omega^2 - (k+\kappa)]^2 + \kappa^2}{[\gamma^2\omega^2 + (\omega^2 - k)^2]\{\gamma^2\omega^2 + [\omega^2 - (k+2\kappa)]^2\}}, \tag{21}$$

$$L_{12} = \left(\frac{T\kappa\omega}{2}\right)\frac{2\gamma\omega(\kappa + k - \omega^2)\cos(\delta\omega) - \{\gamma^2\omega^2 - [\omega^2 - (k+\kappa)]^2 + \kappa^2\}\sin(\delta\omega)}{[\gamma^2\omega^2 + (\omega^2 - k)^2]\{\gamma^2\omega^2 + [\omega^2 - (k+2\kappa)]^2\}}, \tag{22}$$

$$L_{21} = \left(\frac{T\kappa\omega}{2}\right)\frac{2\gamma\omega(\kappa + k - \omega^2)\cos(\delta\omega) + \{\gamma^2\omega^2 - [\omega^2 - (k+\kappa)]^2 + \kappa^2\}\sin(\delta\omega)}{[\gamma^2\omega^2 + (\omega^2 - k)^2]\{\gamma^2\omega^2 + [\omega^2 - (k+2\kappa)]^2\}}, \tag{23}$$

and

$$L_{TT} = \overline{\kappa}T^2, \tag{24}$$

respectively. All other Onsager coefficients are zero. We pause to make some comments: First, for $\Delta T = 0$, expressions for L_{ij} ($i = 1$ and 2) are exact and valid for arbitrary large values of f_i's. Second, one can verify that $L_{11} = L_{22} \geqslant 0$ and $(L_{12} + L_{21})^2 \leqslant 4L_{11}L_{22}$ in agreement with the second law of thermodynamics. The above conditions are promptly verified for all k, κ and ω. The nondiagonal Onsager coefficients L_{12} and L_{21} are not the same, except for the lagless case $\delta = 0$. Third, in the regime of low and large frequencies, all coefficients behave as ω^2 and $1/\omega^2$ (diagonal) and $1/\omega^4$ (nondiagonal for $\delta = 0$), respectively. Fourth, the nondiagonal coefficients vanish for sufficiently weak interactions while the diagonal is finite, consistent with a quasidecoupling between particles. Conversely, when the coupling parameter is very strong, $\kappa \to \infty$, all coefficients remain finite and coincide with those for one Brownian particle in a harmonic potential subjected to both external forces. Fifth, for large ΔT, Eq. (16) states that the heat exchanged with the thermal bath i has two contributions: the first, coming from external forces, has the form $A_i f_i^2 + B_i f_i f_j + C_i f_j^2$ (with coefficients A_i, B_i, and C_i listed in Appendix B) and it is strictly non-negative. Hence, coefficients satisfy $A_i \geqslant 0$ and $C_i \geqslant 0$ and $B_i^2 - 4A_iC_i \leqslant 0$. The second term, coming from the difference of temperatures, can be positive or negative depending on the sign of $T_j - T_i$. In the absence of external forces, the entropy production reduces to Eq. (18). Sixth, expressions for coefficients $\tilde{L}_{ij}$'s appearing in Eq. (19) (see Appendix B) are exact and hold beyond linear regime listed (large forces and/or large difference of

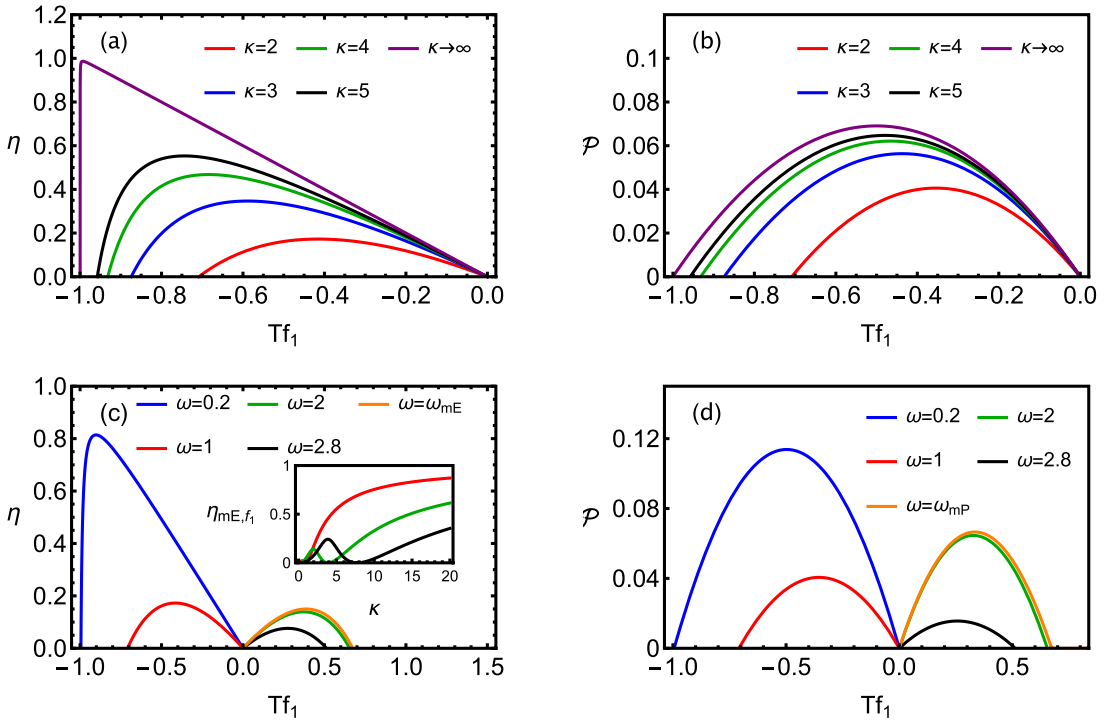

FIG. 2. For the work-to-work regime, panels (a) and (b) depict the efficiency η and power output $\mathcal{P}$ vs strength force $X_1 = T f_1$ for distinct interaction strengths κ's and $\omega = 1$. In (c) and (d), the same but for distinct ω's and $\kappa = 2$. Inset: Maximum efficiency η_{mE,f_1} vs κ for distinct ω's. In all cases, we set $X_2 = T f_2 = 1$, $T = 0.3$, $\delta = 0$, and $k = 0.1$.

temperatures) between thermal baths in Appendix B. Seventh and last, the interplay between both terms can change the direction of the heat flowing per cycle, implying that the coupling parameter can change the regime of operation of the engine, from heater to heat engine and vice versa, as κ is increased and decreased. Similar findings have also been observed for two coupled double quantum dots [52] and coupled spins [53].

III. EFFICIENCY

A generic system operates as an engine when parameters are set in such a way that a given amount of energy received is partially converted into power output $\mathcal{P} \geqslant 0$. A measure for the efficiency η is given by the ratio between above quantities and constitutes a fundamental quantity for characterizing such conversion. Our aim here consists of exploring the role of distinct parameters, mainly the interaction between particles, in such a way that such system can operate as an efficient engine. By considering, for instance, the particle $i = 2$ as the work source, the engine regime implies that $\mathcal{P} = \overline{\dot{W}}_1 \geqslant 0$, and according to Eq. (16) the system will receive heat when $T_1 \gg T_2$ ($T_2 \gg T_1$), consistent with $\overline{\dot{Q}}_1 < 0$ ($\overline{\dot{Q}}_2 < 0$). Conversely, when the difference of temperatures between thermal baths is small and/or when forces f_1/f_2 are large, both particles do not necessarily receive heat from the thermal bath and only input work (actually input power) can be converted into output work. Such class of engines, also known as work-to-work converter, will be analyzed next.

We shall split the analysis in the regime of equal and different temperatures. For both cases, we will investigate the machine performance with respect to the loading force f_1 and other parameters, such as interaction κ and phase difference δ.

A. Work-to-work converter

Since for equal temperatures $\overline{\dot{Q}}_1$ and $\overline{\dot{Q}}_2$ are non-negative, consistent with the system solely delivering heat to the thermal baths, Eq. (45) reduces to the ratio between work sources:

$$\eta \equiv -\frac{\mathcal{P}}{\overline{\dot{W}}_2} = -\frac{L_{11} f_1^2 + L_{12} f_1 f_2}{L_{21} f_2 f_1 + L_{22} f_2^2}, \tag{25}$$

where the far-right-hand side of Eq. (25) was reexpressed in terms of Onsager coefficients and thermodynamic forces.

Figure 2 depicts, for $\delta = 0$, the main features of the efficiency and power output by analyzing the influence of interaction κ and frequency ω. We find that the interaction between particles improves substantially the machine performance. Properly tuning κ not only changes the operation regime, from heater to a work-to-work converter (engine), but also increases the power, efficiency and the range of operation [e.g., the possible values of f_1 within the same engine regime; cf. Figs. 2(a) and 2(b)]. Unlike the engine, in the heater operation mode (often called dud engine), work is extracted from both work sources ($\overline{\dot{W}}_1$ and $\overline{\dot{W}}_2 > 0$). For sufficient strong interactions, maximum efficiencies increase toward the ideal limit $\eta_{mE,f_1} \to 1$ achieved as $\kappa \to \infty$ (inset). There are two range of output forces for the engine operation: The former,

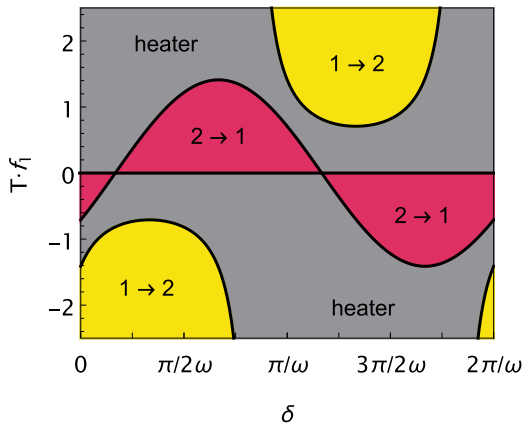

FIG. 3. Phase diagram $X_1 = T f_1$ vs δ for the work-to-work converter. Symbols $1 \to 2/\ 2 \to 1$ and heater correspond to the engine and dud regimes in which there is the conversion from $\dot{\overline{W}}_1 < 0$ into $\dot{\overline{W}}_2 > 0$ and vice versa and $\dot{\overline{W}}_1 > 0$ and $\dot{\overline{W}}_2 > 0$, respectively. Parameters: $X_2 = T f_2 = \gamma = \omega = 1$, $k = 0.1$, $T = 0.3$, and $\kappa = 2$.

for $k + \kappa > \omega^2$, f_1 has opposite direction to f_2 as depicted in Figs. 2(c) and 2(d). The increase of frequency in such case reduces the machine efficiency until it vanishes for $\omega^2 = k + \kappa$. Conversely, f_1 has the same direction as f_2 when $k + \kappa < \omega^2$, and it is marked for there are optimal frequencies ω_{mE} and ω_{mP} ensuring maximum efficiency and power, respectively. The former is given by $\omega_{mE} = \sqrt{k + \kappa + \sqrt{k + \kappa + \kappa^2}}$ with associated efficiency and power given by Eq. (25). Since the expression for ω_{mP} is very lengthy, we shall not show it here. Whenever ω_{mE} is independent on the ratio f_2/f_1, ω_{mP} depends on them. Finally, the engine behaves very inefficiently for $\omega \gg 1$. This can be understood by the fact that the system presents some inertia and does not properly respond to abrupt changes when frequency is large.

Next, we examine the influence of a phase difference between harmonic forces, as depicted in Figs. 3–5. The existence of a lag between driving forces not only controls the power and efficiency, but can also guide the operation modes of the system. In other words, depending on the value of δ, the work is extracted from the work source 1 and dumped into the work source 2 ($\eta = -\dot{\overline{W}}_2/\dot{\overline{W}}_1$) or vice versa ($\eta = -\dot{\overline{W}}_1/\dot{\overline{W}}_2$); both conversions are possible for the same output force or even none of them.

Such changes of conversion in the operation model (see, e.g., Fig. 3) share some similarities with some theoretical models for kinesin in which the range chemical potentials and mechanical forces can rule the energy conversion (chemical into mechanical and vice versa) [3].

Now that we have introduced the main features about the model parameters and how they influence the machine performance, we are going to present distinct protocols for optimizing them.

1. Maximization with respect to the output force

The first (and simplest) maximization is carried out with respect to the output force f_1 and the other parameters are held fixed. Such optimizations have been performed in Refs. [14,29]. Since $\mathcal{P} = \dot{\overline{W}}_1 \geqslant 0$ the engine regime is delimited by the interval $0 \leqslant |f_1| \leqslant |f_m|$ where $f_m \equiv -L_{12} f_2/L_{11}$. By adjusting the output forces f_{1mP} and f_{1mE} ensuring maximum power $\mathcal{P}_{mP,f_1}$ (with efficiency η_{mP,f_1}) and maximum efficiency η_{mE,f_1} (with power $\mathcal{P}_{mE,f_1}$), we obtain the following expressions, expressed in terms of Onsager coefficients [14]:

$$f_{1mE} = \frac{L_{22}}{L_{12}}\left(-1 + \sqrt{1 - \frac{L_{21}L_{12}}{L_{22}L_{11}}}\right) f_2 \tag{26}$$

and

$$f_{1mP} = -\frac{1}{2}\frac{L_{12}}{L_{11}} f_2, \tag{27}$$

respectively, with corresponding efficiencies

$$\eta_{mE,f_1} = -\frac{L_{12}}{L_{21}} + \frac{2L_{11}^2}{L_{21}^2}\left(1 - \sqrt{1 - \frac{L_{21}L_{12}}{L_{11}^2}}\right) \tag{28}$$

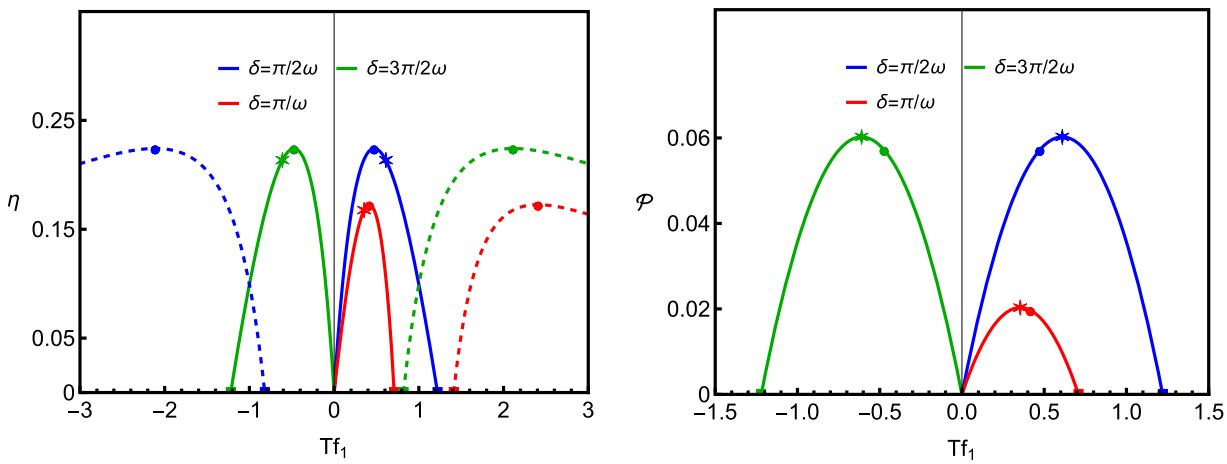

FIG. 4. For the same parameters from Fig. 3, the efficiency η (left) and power output $\mathcal{P}$ (right) vs $X_1 = T f_1$ for distinct phase differences δ's. Dashed and continuous lines correspond to the conversion from $\dot{\overline{W}}_1$ into $\dot{\overline{W}}_2$ and vice versa, respectively. Circles, stars, and squares denote the maximum efficiency, maximum power, and $T f_m$, respectively.

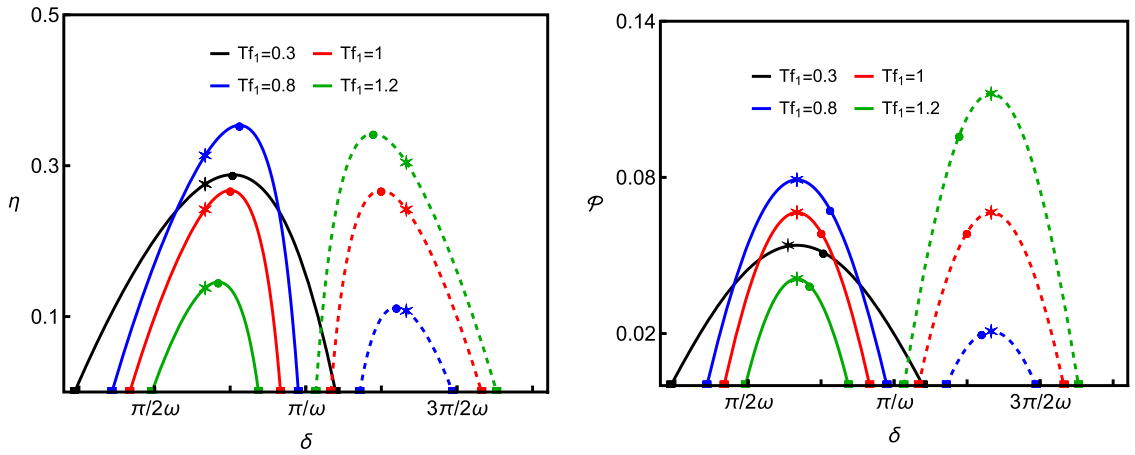

FIG. 5. For the same parameters from Fig. 3, the efficiency η (left) and power output $\mathcal{P}$ (right) vs phase difference δ for distinct $X_1 = Tf_1's$. Continuous and dashed lines correspond to the conversion from $\overline{W}_2$ into $\overline{W}_1$ and vice versa, respectively. Squares, stars, and circles denote the δ_{m1}/δ_{m2}, maximum power, and maximum efficiency, respectively.

and

$$\eta_{mP,f_1} = \frac{L_{12}^2}{4L_{11}^2 - 2L_{21}L_{12}}, \tag{29}$$

respectively, where the property $L_{22} = L_{11}$ has been used. Similar expressions are obtained for $\mathcal{P}_{mE,f_1}$ and $\mathcal{P}_{mP,f_1}$ by inserting f_{1mE} and f_{1mP} into the relation for $\mathcal{P}$. Maximum efficiencies are not independent from each other, but related via the simple relation

$$\eta_{mP,f_1} = \frac{P_{mP,f_1}}{2P_{mP,f_1} - P_{mE,f_1}}\eta_{mE,f_1}, \tag{30}$$

respectively [14]. Expressions for maximum quantities are depicted in Fig. 4 and Fig. 6 (continuous lines).

2. *Maximization with respect to the interaction or phase difference between harmonic forces*

Here we present an alternative route for improving the engine performance, based on optimal choices of κ or δ. Since both of them appear only in Onsager coefficients, their maximizations are described by common set of relations, when expressed in terms of Onsager coefficients. Let α_{mP} and α_{mE} be the optimal parameter (κ or δ) which maximize the power output and efficiency, respectively. From expressions for $\mathcal{P}$ and η, their values are given by

$$f_1 = -\frac{L'_{12}(\alpha_{mP})}{L'_{11}(\alpha_{mP})}f_2 \tag{31}$$

and

$$f_1 = \left(\frac{-B(\alpha_{mE}) \pm \sqrt{B^2(\alpha_{mE}) - 4A(\alpha_{mE})C(\alpha_{mE})}}{2A(\alpha_{mE})}\right)f_2, \tag{32}$$

respectively, where parameters A, B, and C are given by

$$A(\alpha_{mE}) = L'_{11}(\alpha_{mE})L_{21}(\alpha_{mE}) - L_{11}(\alpha_{mE})L'_{21}(\alpha_{mE}), \tag{33}$$

$$B(\alpha_{mE}) = L_{21}(\alpha_{mE})L'_{12}(\alpha_{mE}) - L_{12}(\alpha_{mE})L'_{21}(\alpha_{mE}), \tag{34}$$

and

$$C(\alpha_{mE}) = L_{22}(\alpha_{mE})L'_{12}(\alpha_{mE}) - L_{12}(\alpha_{mE})L'_{22}(\alpha_{mE}), \tag{35}$$

respectively, where $L'_{ij}(\alpha) \equiv \partial L_{ij}/\partial\alpha$ denotes the derivative of coefficient L_{21} evaluated at α_{mP} and α_{mE} and the property $L_{22} = L_{11}$ was again used to derive Eq. (32). The corresponding $\mathcal{P}_{mP,\alpha}/\eta_{mP,\alpha}$ is straightforwardly evaluated and given by

$$\mathcal{P}_{mP,\alpha} = \frac{TL'_{12}(\alpha_{mP})}{L'^2_{11}(\alpha_{mP})}[L_{12}(\alpha_{mP})L'_{11}(\alpha_{mP}) - L_{11}(\alpha_{mP})L'_{12}(\alpha_{mP})]f_2^2, \tag{36}$$

$$\eta_{mP,\alpha} = \frac{L'_{12}(\alpha_{mP})[L_{12}(\alpha_{mP})L'_{11}(\alpha_{mP}) - L_{11}(\alpha_{mP})L'_{12}(\alpha_{mP})]}{L'_{11}(\alpha_{mP})[L_{22}(\alpha_{mP})L'_{11}(\alpha_{mP}) - L_{21}(\alpha_{mP})L'_{12}(\alpha_{mP})]}, \tag{37}$$

respectively, and similar expressions are obtained for $\mathcal{P}_{mE,\alpha}$ and $\eta_{mE,\alpha}$ by inserting Eq. (32) into expressions for $\mathcal{P}$ and η. By focusing on the maximization with respect to the phase difference, we see that the engine regime is delimited by two values of δ_{m1} and δ_{m2} in which $\mathcal{P} \geqslant 0$. From the above expressions, the maxima δ_{mP} and δ_{mE} are given by

$$\delta_{mP} = \frac{1}{\omega}\tan^{-1}\left\{\frac{-k^2 - 2k(\kappa - \omega^2) + \omega^2[2\kappa - (\omega^2 - \gamma^2)]}{2\gamma\omega(-\kappa - k + \omega^2)}\right\}, \tag{38}$$

and

$$\frac{f_1}{f_2} = \frac{B(\delta_{mE})}{2L'_{21}(\delta_{mE})L_{11}}\left[1 \mp \sqrt{1 + \frac{4L_{11}^2L'_{21}(\delta_{mE})L'_{12}(\delta_{mE})}{B^2(\delta_{mE})}}\right], \tag{39}$$

respectively. We pause again to make some few comments: First, since the lag appears only in crossed Onsager coefficients, the optimal δ_{mP} does not depend on forces f_1/f_2, solely depending on γ, k, κ, and ω [see, e.g., dashed lines in Fig. 6(b)]. Second, for $k + \kappa \gg \omega^2$ and $k + \kappa \ll \omega^2$, the optimal $\omega\delta_{mP} \to \pi/2$ and $-\pi/2$, respectively. Third, in contrast with δ_{mP}, δ_{mE} depends on ratio f_2/f_1 [see, e.g., dashed lines in Fig. 6(a)], and its value is given by the solution of transcendental Eq. (39). Figure 5 exemplifies the maximiza-

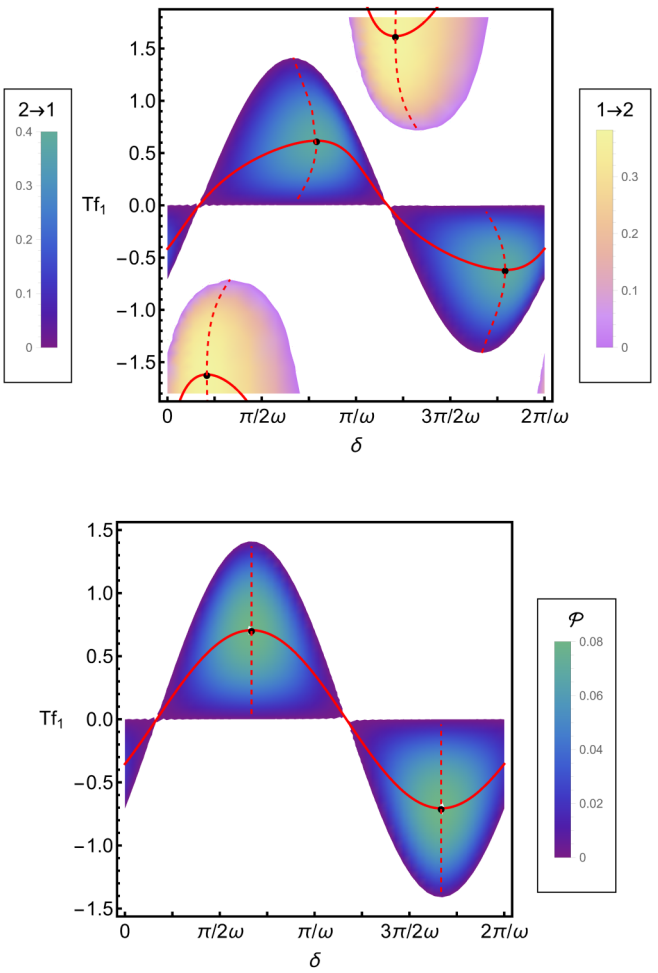

FIG. 6. For the same parameters from Fig. 3, depiction of efficiency (top) and power output (bottom) for distinct Tf_1 and δ. Continuous and dashed lines denote the maximization with respect to the force f_1 and δ, respectively. The intersection between curves corresponds to the simultaneous maximization (circle).

tion of engine with respect to the phase difference for some values of output forces, and Fig. 6 shows (dashed lines), for several f_1 and δ', the power and efficiency associated with the conversion from $\overline{\dot{W}}_2$ into $\overline{\dot{W}}_1$ and vice versa.

3. Complete maximization of engine

Here we address the optimization with respect to the output force and lag simultaneously. In other words, the maximum power output and efficiency must satisfy simultaneously Eqs. (27) and (38) and Eqs. (26) and (39), respectively. Starting with the power output, the existence of an optimal lag δ^*_{mP} and f^*_{1mP} implies that

$$\frac{L'_{12}(\delta^*_{mP})}{L'_{11}(\delta^*_{mP})} = \frac{1}{2}\frac{L_{12}(\delta^*_{mP})}{L_{11}(\delta^*_{mP})} \tag{40}$$

and

$$f^*_{1mP} = -\frac{1}{2}\frac{L_{12}(\delta^*_{mP})}{L_{11}(\delta^*_{mP})} f_2, \tag{41}$$

respectively. Expressions for power and efficiency at maximum power at simultaneous maximizations are readily evaluated and given by

$$\mathcal{P}^*_{mP} = \frac{T}{4}\frac{L^2_{12}(\delta^*_{mP})}{L_{11}(\delta^*_{mP})} f_2^2 \tag{42}$$

and

$$\eta^*_{mP} = \frac{L^2_{12}(\delta^*_{mP})}{4L^2_{11}(\delta^*_{mP}) - 2L_{12}(\delta^*_{mP})L_{21}(\delta^*_{mP})}. \tag{43}$$

Similar expressions for the global maximum efficiency and power at maximum efficiency are obtained by inserting f^*_{1mE}/δ^*_{mE} into the expression for power and efficiency, respectively, the former being given by

$$\eta^*_{mE} = -\frac{L_{12}(\delta^*_{mE})}{L_{21}(\delta^*_{mE})} + \frac{2L^2_{11}(\delta^*_{mE})}{L^2_{21}(\delta^*_{mE})} \times \left[1 - \sqrt{1 - \frac{L_{21}(\delta^*_{mE})L_{12}(\delta^*_{mE})}{L^2_{11}(\delta^*_{mE})}}\right], \tag{44}$$

respectively.

Figure 6 depicts the simultaneous maximization of power and efficiency with respect to the phase difference and output force for the same parameters from Fig. 3. For the sake of comparison, we also look a the lagless case are depicted in Figs. 2(a) and 2(b). Although the engine operates rather inefficiently for $\delta = 0$ (maximum efficiency and power read $\eta_{mE} \approx 0.172$ and $\mathcal{P}_{mP} \approx 0.020$, respectively) the simultaneous maximization of engine provides a substantial increase of power and output, reading $\eta^*_{mE} \approx 0.382$ and $\mathcal{P}^*_{mP} \approx 0.081$. Similar findings are obtained for other values of κ and ω, in which the machine performance increases by raising κ and lowering ω.

B. Different temperatures

In this section, we derive general findings for the case of each particle placed in contact with a distinct thermal bath. We shall restrict our analysis for $k + \kappa > \omega^2$, where the efficiency is expected to be larger. Although the power output $\mathcal{P}$ is the same as before, the efficiency may change due to the appearance of heat flow, and therefore its maximization will occur (in general) for distinct output forces and phase differences when compared with the work-to-work converter. The efficiency η in such case then reads

$$\eta = -\frac{\mathcal{P}}{\overline{\dot{W}}_2 + \overline{\dot{Q}}_i}. \tag{45}$$

Contrasted with the work-to-work converter, in which particles dump heat only to the reservoirs [and hence the heat is not considered in Eq. (25)], the temperature difference may be responsible for some amount of heat flowing from the reservoirs to the system). The difference in temperature affects the particle's velocity fluctuations but does not change its average $\langle v_i \rangle$, therefore the output power $\mathcal{P}$ is unaffected by ΔT [cf. Eq. (B7)], the efficiency will always decrease as the temperature gap is raised. For a small difference of temperatures, the heat regime occurs for a lower range of f_1 or δ than the entire engine regime, since $Q_i \leqslant 0$ only for some specific parameters. In other words, let f_h the threshold force separating both

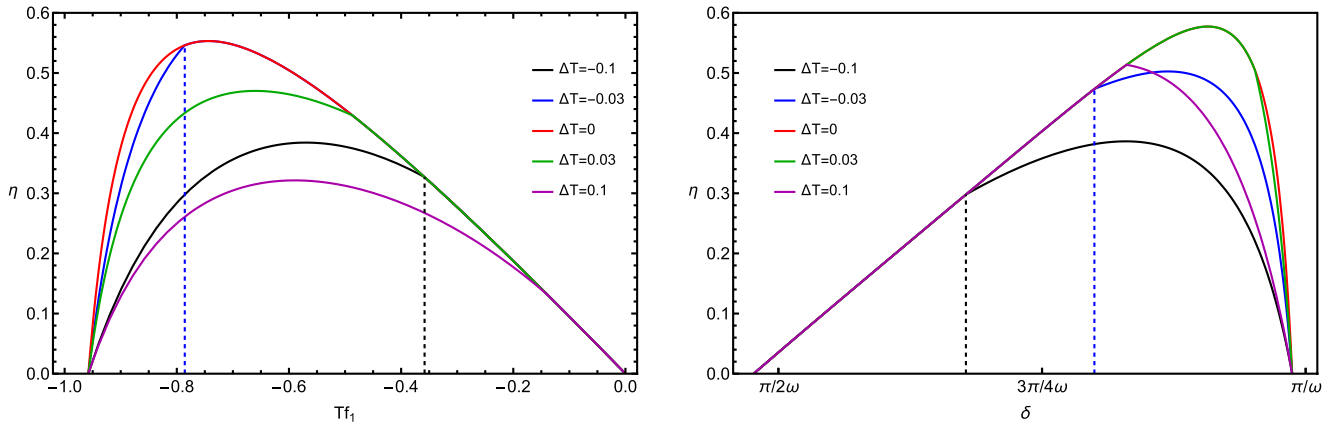

FIG. 7. For distinct temperature reservoirs, left and right panels depict the efficiency vs Tf_1 (for $\delta = 0$) and vs δ (for $Tf_1 = 1$), respectively. The vertical lines denote the values of f_h and δ_h separating the operation regimes. The red curves show the work-to-work efficiency. Parameters: $T = 0.3 + \Delta T/2$, $\omega = 1$, $k = 0.1$, $\kappa = 5$, and $Tf_2 = 1$.

operation regimes (an analogous description holds valid for δ_h). For $|f_h| < |f_1| \leqslant |f_m|$ the engine receives heat from one thermal bath, since $\overline{\dot{Q}}_i < 0$ or equivalently $\overline{\kappa}\Delta T - B_i f_i f_j > A_i f_i^2 + C_i f_j^2$. The force f_h then satisfies $\overline{\dot{Q}}_i(f_h) = 0$, or equivalently $C_i f_h^2 + A_i f_i^2 = \overline{\kappa}\Delta T - B_i f_i f_h$. For $0 \leqslant |f_1| \leqslant |f_h|$, the machine then works as a work-to-work converter, and therefore the temperature difference is playing no role (results from Sec. III A are held valid in this case). It is worth mentioning that above inequality can be satisfied under distinct ways: for large ΔT and/or choices of δ or f_1.

Despite all calculations being exact, expressions for the efficiency and their maximizations become more involved, since they also depend on coefficients A_i, B_i, and C_i. In order to obtain some insights about its behavior in the presence of a heat flux, let us perform an analysis for $\Delta T \ll 1$ and $\Delta T \gg 1$. In the former limit, η is approximately given by $\eta \approx -(\overline{\dot{W}}_1/\overline{\dot{W}}_2)(1 - \overline{\dot{Q}}_i/\overline{\dot{W}}_2)$. By expressing it in terms of Onsager coefficients, one arrives at the following approximate expression for the efficiency:

$$\eta \approx -\frac{L_{11}f_1^2 + L_{12}f_1 f_2}{L_{22}f_2^2 + L_{12}f_2 f_1}\left[1 + \frac{\overline{\dot{Q}}_i}{T(L_{22}f_2^2 + L_{21}f_2 f_1)}\right], \quad (46)$$

where the input heat $\overline{\dot{Q}}_i < 0$ plays the role of decreasing the efficiency. Maximizations with respect to f_1 and δ can be carried out from above (approximate) expression if $|f_{mE}| \geqslant |f_h|$ and $\delta_{mE} > \delta_h$ and from Eq. (26) if $|f_{mE}| \leqslant |f_h|$ and $\delta_{mE} \leqslant \delta_h$.

For the opposite limit $\Delta T \gg 1$, the efficiency is approximately given by $\eta \approx -T(L_{12}f_1 f_2 + L_{11}f_1^2)/\overline{\kappa}\Delta T$, revealing that η decreases asymptotically as ΔT^{-1} for large temperature differences. Recalling that the numerator does not depend on the temperature (see, e.g., Appendix B), it is clear that $\eta \ll 1$, with maximum values η_{mE} and $\eta_{mE,\delta}$ given by $\eta_{mE} \approx \mathcal{P}_{mP}/\overline{\kappa}\Delta T$ and $\eta_{mE,\delta} \approx \mathcal{P}_{mP,\delta}/\overline{\kappa}\Delta T$ for f_{1mP} and δ_{mP}, respectively. For an intermediate ΔT, the system receives heat from the hot thermal bath along $0 < |f_1| < |f_m|$ or $\delta_{m1} \leqslant \delta \leqslant \delta_{m2}$, both maximizations are straightforwardly calculated from Eq. (45). Analogous relations are obtained for $T_i < T_j$ by replacing $\overline{\dot{Q}}_i$ for $\overline{\dot{Q}}_j$.

In order to illustrate above findings, Fig. 7 exemplifies the efficiency for distinct and small $\Delta T = T_2 - T_1$ for fixed $\delta = 0$ (left panel) and $f_1 = 1$ (right panel). As stated before, the power $\mathcal{P}$ is the same as in Fig. 2(b) for $\kappa = 5$. Since $\overline{\dot{Q}}_1$ and $\overline{\dot{Q}}_2$ exhibit distinct dependencies with f_1 and δ, the amount of heat received will be different when $\Delta T > 0$ or <0. Such findings depict that it can more advantageous to receive heat from the thermal bath 1 or 2 depending on the parameters the machine is projected. Such advantages are examined in more details in Fig. 8, in which we extend for lower interaction parameter and several values of f_1 and δ for $\Delta T = 0.3$ and -0.3. As for the work-to-work converter, there is also the global maximization corresponding to the intersection between both maximum lines. Since the efficiency is lower than the work-to-work converter (see, e.g., Fig. 6), the role of the present optimization (whether with respect f_1, δ or both) is revealed to be relevant for enhancing the engine performance.

IV. CONCLUSIONS

In this paper, we introduced and analyzed a model for a small-scale engine based on interacting Brownian particles subject to periodically driving forces. General expressions for the thermodynamic properties, power output, and efficiency were investigated. Interaction between particles plays a central role not only for improving the machine performance but also for changing the machine regime operation. Furthermore, we observe the existence of distinct operation regimes for the same driving strength or phase difference. The present framework is revealed to be a suitable route for obtaining efficient thermal engines that benefit from interactions and may constitute a first step for the description of larger chains of interacting particles.

Although we here focused on the interaction between particles as an alternative and reliable route for optimizing the machine performance, it is worth mentioning that this method can be combined with other optimization methods known in the literature (see, e.g., Refs. [32,43–46]). Whenever an upper limit for efficiency and power is obtained for a given frequency, our engine can achieve a larger performance by choosing a suitable (large) interaction between particles. It is

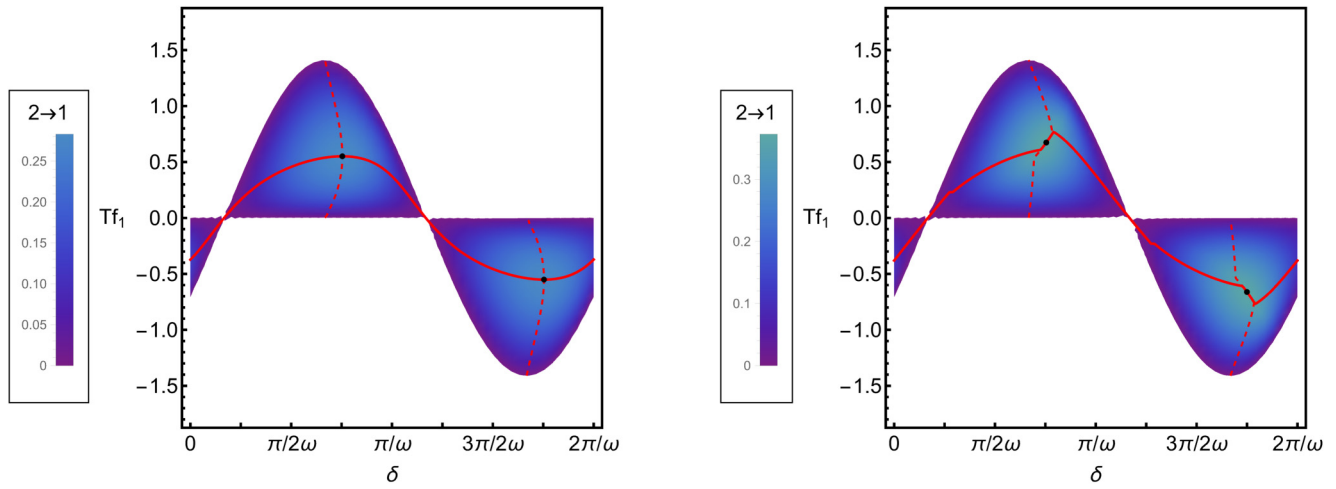

FIG. 8. For the same parameters from Fig. 6, left and right panels depict of efficiency (for the conversion from $\overline{\dot{W}}_2$ into $\overline{\dot{W}}_1$) as a function of Tf_1 and δ for $\Delta T = -0.3$ and 0.3, respectively. Continuous and dashed lines denote the maximization with respect to the force Tf_1 and δ, respectively. The simultaneous maximization (circles) corresponds to the intersection between maximum curves.

also worth noting that in the case of infinitely strong coupling, $\kappa \to \infty$, our results reduce to those of a single particle with two external forces [17].

It would be interesting to see whether the results of this paper can be extended to systems with more than two particles, with arbitrary interaction strengths. Furthermore, it is worth noting that, at constant temperature, our system can be mapped on a general Ornstein-Uhlenbeck process [54]. It would be interesting to see whether this mapping can be extended to systems with different temperatures, such as the ones studied in this paper.

It is worth pointing out that positions and velocities get uncoupled for the sort of drivings we have considered and thereby the heat received by the particle can not be converted into useful work. Hence, an interesting extension of the present work would be to exploit other kinds of time-dependent drivings providing the heat to be converted into useful work. Another potential extension of our work would be to study engines composed of chains of larger systems sizes, in order to compare the role of system size for enhancing the efficiency and power.

ACKNOWLEDGMENTS

The authors acknowledge financial support from the São Paulo Research Foundation (FAPESP) under Grants No. 2020/12021-6, No. 2017/24567-0, No. 2020/03708-8, No. 2018/02405-1, and No. 2021/03372-2.

APPENDIX A: EXPRESSIONS FOR COVARIANCES

From the Fokker-Planck-Kramers equation, the time evolution of covariances $b_{ij}^{xv}(t) \equiv \langle x_i v_j \rangle(t) - \langle x_i \rangle(t) \langle v_j \rangle(t)$ is given by

$$\frac{db_{11}^{xx}}{dt} = 2b_{11}^{xv}, \tag{A1}$$

$$\frac{db_{11}^{vv}}{dt} = -2(k+\kappa)b_{11}^{xv} + 2\kappa b_{12}^{xv} - 2\gamma b_{11}^{vv} + 2\gamma T_1, \tag{A2}$$

$$\frac{db_{11}^{xv}}{dt} = b_{11}^{vv} - (k+\kappa)b_{11}^{xx} + \kappa b_{12}^{xx} - \gamma b_{11}^{xv}, \tag{A3}$$

$$\frac{db_{12}^{xx}}{dt} = b_{12}^{xv} + b_{21}^{xv}, \tag{A4}$$

$$\frac{db_{12}^{vv}}{dt} = -(k+\kappa)\left(b_{12}^{xv} + b_{21}^{xv}\right) + \kappa\left(b_{11}^{xv} + b_{22}^{xv}\right) - 2\gamma b_{12}^{vv}, \tag{A5}$$

and

$$\frac{db_{12}^{xv}}{dt} = b_{12}^{vv} - (k+\kappa)b_{12}^{xx} + \kappa b_{11}^{xx} - \gamma b_{12}^{xv}, \tag{A6}$$

respectively, and analogous relations are obtained for $b_{21}^{xx}, b_{21}^{vv}, b_{21}^{xv}$ and $b_{22}^{xx}, b_{22}^{vv}, b_{22}^{xv}$ just by replacing $1 \leftrightarrow 2$. From the above set of linear equations, all expressions for steady-state covariances are obtained, as listed here. Since only b_{ij}^{vv} are needed for obtaining the entropy production, we shall omit their expressions, but they can be found in Ref. [48].

APPENDIX B: EXPRESSIONS FOR THE ENTROPY PRODUCTION, AVERAGE WORK, AND HEAT OVER A COMPLETE CYCLE

In this Appendix, we list the main expressions for $\overline{\dot{W}}_1$, $\overline{\dot{W}}_2\overline{\dot{Q}}_1$, $\overline{\dot{Q}}_2$ and $\overline{\sigma}$ averaged over a complete cycle. As stated previously, our starting point are the relationships $\dot{W}_i = -mF_i(t)\langle v_i \rangle$ and $\dot{Q}_i = \gamma(m\langle v_i^2 \rangle - k_B T_i)$ together averages $\langle v_i \rangle$ and $\langle v_i \rangle^2$ integrated over a complete cycle.

The steady-state entropy production given by the expression

$$\overline{\sigma} = \frac{\overline{\dot{Q}}_1}{T_1} + \frac{\overline{\dot{Q}}_2}{T_2}, \tag{B1}$$

which is a sum of two terms: Φ_T and $\overline{\Phi}_f$. Thelatter one, due to the external forces, has the form $\tilde{L}_{11}X_1^2 + (\tilde{L}_{12} + \tilde{L}_{21})X_1X_2 + \tilde{L}_{22}X_2^2$, where coefficients (for $m = k_B = 1$) are given by

$$\tilde{L}_{11} = \frac{\gamma\omega^2}{T_1T_2}\frac{T_1\kappa^2 + T_2\{(k+\kappa)^2 + \omega^2[\gamma^2 + \omega^2 - 2(k+\kappa)]\}}{[\gamma^2\omega^2 + (\omega^2 - k)^2][\gamma^2\omega^2 + (\omega^2 - k - 2\kappa)^2]}, \tag{B2}$$

$$\tilde{L}_{12} + \tilde{L}_{21} = \frac{\gamma\omega^2\kappa}{2T_1T_2}\frac{(T_1 + T_2)(k + \kappa - \omega^2)\cos(\delta\omega) + (T_1 - T_2)\gamma\omega\sin(\delta\omega)}{[\gamma^2\omega^2 + (\omega^2 - k)^2][\gamma^2\omega^2 + (\omega^2 - k - 2\kappa)^2]}, \tag{B3}$$

and

$$\tilde{L}_{22} = \frac{\gamma\omega^2}{T_1T_2}\frac{T_2\kappa^2 + T_1\{(k+\kappa)^2 + \omega^2[\gamma^2 + \omega^2 - 2(k+\kappa)]\}}{[\gamma^2\omega^2 + (\omega^2 - k)^2][\gamma^2\omega^2 + (\omega^2 - k - 2\kappa)^2]}, \tag{B4}$$

respectively. Note that above coefficients reduce to Onsager coefficients L_{21} when $T_1 = T_2$.

In order to relate coefficients $\tilde{L}_{ij}$ with Onsager ones L_{ij}, it is convenient to expand Eq. (17) in the regime of small ΔT, in such a way that $\overline{\sigma}$ is approximately given by

$$\overline{\sigma} \approx \left[-\frac{1}{T}(\overline{\dot{W}}_1 + \overline{\dot{W}}_2) + (\overline{\dot{Q}}_1 - \overline{\dot{Q}}_2)\frac{\Delta T}{2T^2}\right]. \tag{B5}$$

Since the dependence with ΔT is present only in the far-right-hand term, it is clear that Onsager coefficients L_{ij} $(i, j \in 1, 2)$ correspond to zeroth-order coefficients obtained from the expansion of $\overline{\sigma}$. For this reason, the coefficient $\tilde{L}_{ij}$ can be decomposed as $\tilde{L}_{ij} = L_{ij} + L_{ij}^{(c)}\Delta T$, where $L_{ij}^{(c)}$ is the first-order correction, and then $\overline{\sigma}$ is given by

$$\overline{\sigma} \approx L_{11}f_1^2 + (L_{12} + L_{21})f_1f_2 + L_{22}f_2^2 + \left[L_{11}^{(c)}f_1^2 + \left(L_{12}^{(c)} + L_{21}^{(c)}\right)f_1f_2 + L_{22}^{(c)}f_2^2\right]\Delta T + L_{TT}f_T^2, \tag{B6}$$

where $L_{TT} = \overline{\kappa}T^2 > 0$ with $f_1 = X_1/T$, $f_2 = X_2/T$ and $f_T = \Delta T/T^2$ [where $T = (T_1 + T_2)/2$]. As analyzed in Sec. II, for small ΔT and f_i, the difference between L_{ij} and $\tilde{L}_{ij}$ can be neglected and the entropy production is approximately given by $\overline{\sigma} \approx L_{11}f_1^2 + (L_{12} + L_{21})f_1f_2 + L_{22}f_2^2 + L_{TT}f_T^2$.

The averaged expressions for $\overline{\dot{W}}_1$, $\overline{\dot{W}}_2$, $\overline{\dot{Q}}_1$, and $\overline{\dot{Q}}_2$ are given by

$$\begin{aligned}\overline{\dot{W}}_1 = &-\frac{T^2\gamma\omega^2\{\gamma^2\omega^2 + [\omega^2 - (k+\kappa)]^2 + \kappa^2\}}{2[\gamma^2\omega^2 + (\omega^2 - k)^2]\{\gamma^2\omega^2 + [\omega^2 - (k+2\kappa)]^2\}}f_1^2 \\ &- \frac{T^2\kappa\omega}{2}\frac{2\gamma\omega(\kappa + k - \omega^2)\cos(\delta\omega) - \sin(\delta\omega)\{\gamma^2\omega^2 - [\omega^2 - (k+\kappa)]^2 + \kappa^2\}}{[\gamma^2\omega^2 + (\omega^2 - k)^2]\{\gamma^2\omega^2 + [\omega^2 - (k+2\kappa)]^2\}}f_1f_2,\end{aligned} \tag{B7}$$

$$\begin{aligned}\overline{\dot{W}}_2 = &-\frac{T^2\gamma\omega^2\{\gamma^2\omega^2 + [\omega^2 - (k+\kappa)]^2 + \kappa^2\}}{2[\gamma^2\omega^2 + (\omega^2 - k)^2]\{\gamma^2\omega^2 + [\omega^2 - (k+2\kappa)]^2\}}f_2^2 \\ &- \frac{T^2\kappa\omega}{2}\frac{2\gamma\omega(\kappa + k - \omega^2)\cos(\delta\omega) + \sin(\delta\omega)\{\gamma^2\omega^2 - [\omega^2 - (k+\kappa)]^2 + \kappa^2\}}{[\gamma^2\omega^2 + (\omega^2 - k)^2]\{\gamma^2\omega^2 + [\omega^2 - (k+2\kappa)]^2\}}f_1f_2,\end{aligned} \tag{B8}$$

where

$$\begin{aligned}\overline{\dot{Q}}_1 = &\frac{T^2\gamma\omega^2[\gamma^2\omega^2 + (\kappa + k - \omega^2)^2]}{2[\gamma^2\omega^2 + (k - \omega^2)^2][\gamma^2\omega^2 + (2\kappa + k - \omega^2)^2]}f_1^2 + \frac{T^2\gamma\kappa^2\omega^2}{2[\gamma^2\omega^2 + (k - \omega^2)^2][\gamma^2\omega^2 + (2\kappa + k - \omega^2)^2]}f_2^2 \\ &+ \frac{T^2\gamma\kappa\omega^2[\cos(\delta\omega)(\kappa + k - \omega^2) - \gamma\omega\sin(\delta\omega)]}{[\gamma^2\omega^2 + (k - \omega^2)^2][\gamma^2\omega^2 + (2\kappa + k - \omega^2)^2]}f_1f_2 + \frac{\gamma\kappa^2}{2[\gamma^2k + \kappa(\kappa + \gamma^2)]}\Delta T\end{aligned} \tag{B9}$$

and

$$\begin{aligned}\overline{\dot{Q}}_2 = &\frac{T^2\gamma\kappa^2\omega^2}{2[\gamma^2\omega^2 + (k - \omega^2)^2][\gamma^2\omega^2 + (2\kappa + k - \omega^2)^2]}f_1^2 + \frac{T^2\gamma\omega^2[\gamma^2\omega^2 + (\kappa + k - \omega^2)^2]}{2[\gamma^2\omega^2 + (k - \omega^2)^2][\gamma^2\omega^2 + (2\kappa + k - \omega^2)^2]}f_2^2 \\ &+ \frac{T^2\gamma\kappa\omega^2[\cos(\delta\omega)(\kappa + k - \omega^2) + \gamma\omega\sin(\delta\omega)]}{[\gamma^2\omega^2 + (k - \omega^2)^2][\gamma^2\omega^2 + (2\kappa + k - \omega^2)^2]}f_1f_2 - \frac{\gamma\kappa^2}{2[\gamma^2k + \kappa(\kappa + \gamma^2)]}\Delta T,\end{aligned} \tag{B10}$$

respectively.

[1] U. Seifert, Rep. Prog. Phys. **75**, 126001 (2012).
[2] S. Liepelt and R. Lipowsky, Phys. Rev. Lett. **98**, 258102 (2007).
[3] S. Liepelt and R. Lipowsky, Phys. Rev. E **79**, 011917 (2009).
[4] G. E. Crooks, Phys. Rev. E **60**, 2721 (1999).
[5] C. Jarzynski, Phys. Rev. Lett. **78**, 2690 (1997).
[6] A. C. Barato and U. Seifert, Phys. Rev. Lett. **114**, 158101 (2015).
[7] P. Pietzonka, A. C. Barato, and U. Seifert, Phys. Rev. E **93**, 052145 (2016).
[8] A. C. Barato, R. Chetrite, A. Faggionato, and D. Gabrielli, New J. Phys. **20**, 103023 (2018).
[9] A. Barato, R. Chetrite, A. Faggionato, and D. Gabrielli, J. Stat. Mech. (2019) 084017.
[10] K. Proesmans and C. Van den Broeck, Europhys. Lett. **119**, 20001 (2017).
[11] P. E. Harunari, C. E. Fiore, and K. Proesmans, J. Phys. A: Math. Theor. **53**, 374001 (2020).
[12] Y. Hasegawa and T. Van Vu, Phys. Rev. E **99**, 062126 (2019).
[13] T. Van Vu and Y. Hasegawa, Phys. Rev. Research **2**, 013060 (2020).
[14] K. Proesmans, B. Cleuren, and C. Van den Broeck, Phys. Rev. Lett. **116**, 220601 (2016).
[15] P. Pietzonka and U. Seifert, Phys. Rev. Lett. **120**, 190602 (2018).
[16] V. Blickle and C. Bechinger, Nat. Phys. **8**, 143 (2012).
[17] K. Proesmans, Y. Dreher, M. c. v. Gavrilov, J. Bechhoefer, and C. Van den Broeck, Phys. Rev. X **6**, 041010 (2016).
[18] A. C. Barato and U. Seifert, Phys. Rev. X **6**, 041053 (2016).
[19] K. Proesmans and J. M. Horowitz, J. Stat. Mech. (2019) 054005.
[20] V. Holubec and A. Ryabov, Phys. Rev. Lett. **121**, 120601 (2018).
[21] I. A. Martínez, É. Roldán, L. Dinis, D. Petrov, J. M. Parrondo, and R. A. Rica, Nat. Phys. **12**, 67 (2016).
[22] S. Krishnamurthy, S. Ghosh, D. Chatterji, R. Ganapathy, and A. Sood, Nat. Phys. **12**, 1134 (2016).
[23] P. A. Quinto-Su, Nat. Commun. **5**, 5889 (2014).
[24] P. H. Jones, O. M. Maragò, and G. Volpe, *Optical Tweezers: Principles and Applications* (Cambridge University Press, Cambridge, 2015).
[25] J. A. Albay, G. Paneru, H. K. Pak, and Y. Jun, Opt. Express **26**, 29906 (2018).
[26] A. Kumar and J. Bechhoefer, Appl. Phys. Lett. **113**, 183702 (2018).
[27] G. Paneru and H. Kyu Pak, Adv. Phys.: X **5**, 1823880 (2020).
[28] J. Li, J. M. Horowitz, T. R. Gingrich, and N. Fakhri, Nat. Commun. **10**, 1666 (2019).
[29] A. L. L. Stable, C. E. Fernández Noa, W. G. C. Oropesa, and C. E. Fiore, Phys. Rev. Research **2**, 043016 (2020).
[30] K. Proesmans, C. Driesen, B. Cleuren, and C. Van den Broeck, Phys. Rev. E **92**, 032105 (2015).
[31] S. Rana, P. S. Pal, A. Saha, and A. M. Jayannavar, Phys. Rev. E **90**, 042146 (2014).
[32] T. Schmiedl and U. Seifert, Europhys. Lett. **81**, 20003 (2007).
[33] J. Hoppenau, M. Niemann, and A. Engel, Phys. Rev. E **87**, 062127 (2013).
[34] Z. C. Tu, Phys. Rev. E **89**, 052148 (2014).
[35] P. Chvosta, M. Einax, V. Holubec, A. Ryabov, and P. Maass, J. Stat. Mech. (2010) P03002.
[36] G. Verley, M. Esposito, T. Willaert, and C. Van den Broeck, Nat. Commun. **5**, 4721 (2014).
[37] A. Imparato, L. Peliti, G. Pesce, G. Rusciano, and A. Sasso, Phys. Rev. E **76**, 050101(R) (2007).
[38] C. A. Plata, D. Guéry-Odelin, E. Trizac, and A. Prados, J. Stat. Mech. (2020) 093207.
[39] J. A. Albay, Z.-Y. Zhou, C.-H. Chang, and Y. Jun, Sci. Rep. **11**, 4394 (2021).
[40] Y. Jun, M. c. v. Gavrilov, and J. Bechhoefer, Phys. Rev. Lett. **113**, 190601 (2014).
[41] J.-M. Park, H.-M. Chun, and J. D. Noh, Phys. Rev. E **94**, 012127 (2016).
[42] B. A. N. Akasaki, M. J. de Oliveira, and C. E. Fiore, Phys. Rev. E **101**, 012132 (2020).
[43] F. Curzon and B. Ahlborn, Am. J. Phys. **43**, 22 (1975).
[44] V. Holubec, J. Stat. Mech. (2014) P05022.
[45] P. E. Harunari, F. S. Filho, C. E. Fiore, and A. Rosas, Phys. Rev. Research **3**, 023194 (2021).
[46] N. Golubeva and A. Imparato, Phys. Rev. Lett. **109**, 190602 (2012).
[47] K. Proesmans and C. Van den Broeck, Chaos **27**, 104601 (2017).
[48] T. Tomé and M. J. de Oliveira, Phys. Rev. E **82**, 021120 (2010).
[49] C. Van den Broeck and M. Esposito, Phys. Rev. E **82**, 011144 (2010).
[50] C. E. Fiore and M. J. de Oliveira, Phys. Rev. E **99**, 052131 (2019).
[51] W. A. M. Morgado and D. O. Soares-Pinto, Phys. Rev. E **79**, 051116 (2009).
[52] J. L. D. de Oliveira, M. Rojas, and C. Filgueiras, Phys. Rev. E **104**, 014149 (2021).
[53] X.-L. Huang, X.-Y. Niu, X.-M. Xiu, and X.-X. Yi, Eur. Phys. J. D **68**, 1 (2014).
[54] Y. Tang, R. Yuan, J. Chen, and P. Ao, Phys. Rev. E **91**, 042108 (2015).